The Meteoritical Society

Meteoritics & Planetary Science 42, Nr 7/8, 1417–1427 (2007)
Abstract available online at http://meteoritics.org

A cornucopia of presolar and early solar system materials at the micrometer size range in primitive chondrite matrix

Philip A. BLAND[1, 2*], Frank J. STADERMANN[3], Christine FLOSS[3], Detlef ROST[4], Edward P. VICENZI[4], Anton T. KEARSLEY[2], and Gretchen K. BENEDIX[2]

[1]Impacts and Astromaterials Research Centre (IARC), Department of Earth Science and Engineering, Imperial College London, South Kensington Campus, London SW7 2AZ, UK
[2] IARC, Department of Mineralogy, Natural History Museum, Cromwell Road, London SW7 5BD, UK
[3]Laboratory for Space Sciences and Department of Physics, CB 1105, Washington University, 1 Brookings Drive, Saint Louis, Missouri 63130, USA
[4]Department of Mineral Sciences, National Museum of Natural History, Smithsonian Institution, Washington, D.C. 20560, USA
*Corresponding author. E-mail: p.a.bland@imperial.ac.uk

(Received 02 October 2006; revision accepted 06 April 2007)

Abstract–We have used a variety of complementary microanalytical techniques to constrain the mineralogy, trace-element distributions, and oxygen-isotopic compositions in a 50 × 50 μm area of Acfer 094 matrix. The results reveal the exceptional mineralogical and compositional heterogeneity of this material at the sub-μm level. We observe μm-scale and sub-μm grains with elemental associations suggesting feldspar, metal with widely varying Ni contents, and a Cr-Fe alloy (in addition to forsterite, pyroxene, sulfide, ferrihydrite, and amorphous groundmass previously described). A new class of μm-scale CAI (μCAI) is also observed, which show sub-μm compositional zoning, and a range of oxygen isotopic compositions. Unlike the larger CAIs in Acfer 094, which are uniformly ^{16}O-enriched, two of the three μCAIs we analyzed are isotopically normal. We also observed a Li-rich hotspot that detailed analysis by ToF-SIMS suggests may be a LiCr-oxide grain. Within the resolution of the NanoSIMS, this grain has isotopically normal Li. Finally, in our 50 × 50 μm area, we positively identified a presolar grain that is the most ^{18}O-rich silicate found so far in meteorites. The grain may originate from an asymptotic giant branch (AGB) star, or more likely, a supernova. In line with previous TEM studies (Greshake 1997), we find no evidence for clastic material (e.g., fragmental chondrules) in the matrix of Acfer 094: although the matrix is volatile-depleted, this depletion does not appear to result from dilution of a primordial starting material with (depleted) chondrule fragments. Assuming that matrix experienced the depletion event, our data on the detailed mineralogy of Acfer 094 are currently equivocal in constraining the nature of that event. We observe carrier phases for several elements consistent with conditions approaching equilibrium condensation; however, the presence of an amorphous groundmass is suggestive of more rapid cooling.

INTRODUCTION

Acfer 094 is an ungrouped carbonaceous chondrite that largely escaped thermal and aqueous processing (Newton et al. 1995; Greshake 1997; Nuth et al. 2005). The first detailed petrographic study was by Newton et al. (1995): scanning electron microscopy, transmission electron microscopy, and electron probe were used to study the mineralogy and petrology of chondrules and matrix. These authors calculated that 30–40 vol% of the chondrite consists of grains <10 μm in size. The anhydrous nature of Acfer 094 matrix, the absence of phyllosilicates, and the presence of (~100 nm) forsteritic olivine, enstatitic pyroxene, Fe,Ni sulfides, and amorphous material, were all recognized by these workers. Subsequently, Greshake (1997) used scanning electron microscopy and analytical transmission electron microscopy to study the matrix of Acfer 094. Greshake (1997) also observed only minor serpentine and ferrihydrite, and abundant amorphous material (suggestive of minimal thermal alteration) acting as a groundmass to olivines, pyroxenes, and sulfides. Grain sizes for these phases were typically in the range of 200–400 nm, but smaller grains were also observed (e.g., a class of olivines (Fa < 1), rimmed by material of unknown composition, and 15–80 nm in size).

Based on its texture and composition, Greshake (1997) concluded that the amorphous material formed by disequilibrium condensation in either the cooling solar nebula or a circumstellar environment. Crystalline phases were suggested to have formed either by condensation in the solar nebula or by recrystallization from the amorphous material. Greshake (1997) observed very few clastic grains and explicitly ruled out a chondrule fragmentation origin for the majority of the matrix olivines and pyroxenes (as well as the groundmass amorphous material) on compositional and microstructural grounds. Nuth et al. (2005) also noted the primitive, unaltered nature of Acfer 094, and made comparisons between Acfer 094 matrix and anhydrous IDPs (e.g., both contain abundant amorphous material). Nuth et al. (2005) consider that the similarities may have arisen due to processing in a similar thermal event; they propose chondrule formation as a mechanism for producing amorphous solids and at least some of the crystalline material observed in Acfer matrix.

These previous studies suggest that Acfer 094 matrix may well contain condensed phases—material that is rare or absent in most meteorites (plausibly having been removed by secondary processing). Additional evidence also points to Acfer 094 as a potential host for condensed fines. This meteorite contains an unusually high concentration of presolar grains (Newton et al. 1995), including presolar silicates (Nguyen and Zinner 2004; Mostefaoui and Hoppe 2004; Nagashima et al. 2004; Nguyen et al. 2005; Nguyen et al. 2007). These presolar components of the meteorite matrix have been identified on the basis of their highly anomalous O-isotopic compositions and recent advances in microanalytical technology, most notably the development of the NanoSIMS (Nguyen and Zinner 2004; Mostefaoui and Hoppe 2004; Nguyen et al. 2005; Nguyen et al. 2007). If presolar silicates survived subsequent processing (whether this processing occurred in the nebular or the meteorite parent body), then nebular condensates, which formed later, may also have survived.

The specific environment that produced condensed materials in meteorites and IDPs, and the extent to which condensation influenced chemistry, is the subject of continuing debate, a debate that is inextricably linked to another early solar system process that still awaits a consensus mechanism: volatile depletion. Volatile element fractionation was one of the earliest and most fundamental processes affecting the inner solar nebula. Solids in the inner solar system are depleted in volatile elements compared to solar abundances, with moderately volatile elements showing a monotonic depletion in abundance with decreasing condensation temperature. Models to explain volatile depletion in meteorites and the terrestrial planets fall into one of four categories: a) incomplete condensation during cooling of a hot inner disk, prior to chondrule formation (Wasson and Chou 1974; Wulf et al. 1995; Cassen 1996, 2001); b) two-component models, with volatile depletion occurring during chondrule formation (by evaporation of chondrule melts), and depleted chondrules being mixed with primordial, CI-like matrix (Anders 1964; Shu et al. 1996; Alexander et al. 2001; Alexander 2005); c) evaporative fractionation prior to chondrule formation (Huss et al. 2003); or d) inheritance of a volatile-depleted signature from the ISM (Yin 2004).

Fine-grained matrix is the most primitive major component in chondrites. Analyses of matrix in C2 and C3 chondrites (Bland et al. 2003, 2004, 2005b; Gordon et al. 2007) have revealed that although it is enriched in volatile and moderately volatile elements compared to the bulk meteorite, it does not have a primordial CI-like composition, showing instead a consistent depletion compared to solar in all chondrite groups (except CI). Understanding the mineralogy of the volatile and moderately volatile carrier phases in pristine chondrite matrix would inform our choice of model for volatile depletion. For instance, if volatile depletion occurred by incomplete condensation during slow cooling of a hot inner disk (a), then we might expect a mineralogy that more closely approximates that predicted by equilibrium condensation than might be generated in an environment dominated by the rapid heating and cooling associated with chondrule formation (b). Detailed analysis of fine-grained materials in pristine chondrites has the potential to elucidate not only the mechanism responsible for volatile depletion of course, but also all other processes affecting these materials up to their incorporation into a meteorite parent body. However, matrix is rarely pristine. In addition to nebular processing, fine-grained materials typically experienced variable aqueous, thermal, and impact processing following accretion. Flynn et al. (2004) attempted to overcome this problem by studying trace element carriers in pristine anhydrous IDPs, with a view to constraining nebula condensation models. We have instead chosen to look at matrix in Acfer 094, one of the most pristine chondrites available.

METHODOLOGY

Matrix material in Acfer 094 has previously been analyzed using a variety of microscopy techniques. We used a range of additional instrumentation (LA-ICP-MS, SEM-EDS, ToF-SIMS, and NanoSIMS), to constrain not only the mineralogy, but also trace, minor, and major element abundances and distributions, and isotopic compositions in Acfer 094 matrix, focusing our principal attention on a single 50 × 50 μm^2 area. Data from LA-ICP-MS analysis (performed with a New Wave UP213 laser coupled to a HP7500a ICP-MS at The Open University, UK) of Acfer 094 were first described in Bland et al. (2005b), and analytical methods for this technique are contained therein.

SEM-EDS analyses were performed with a JEOL 5900LV scanning electron microscope operated at high vacuum, fitted with an Oxford Instruments INCA energy dispersive X-ray spectrometer, using an X-sight detector. Accelerating voltage was 20kV and beam current was 2nA. The SEM working distance was 10 mm, and the EDS detector working distance 6 cm.

ToF-SIMS measurements were performed using an ION-TOF TOF SIMS IV instrument at the Smithsonian Institution in Washington, D.C. The pulsed 25 kV Ga^+ primary ion beam enables imaging with a spatial resolution of ~300 nm. Complete mass spectra were collected for every pixel in a 256^2 array; positive and negative secondary ions were collected in successive measurements. The initial overview measurement of 50 × 50 μm^2 was followed by more detailed secondary ion imaging: 20 × 20 μm^2 for presolar grain characterization, and 16 × 16 μm^2 for investigation of a Li-rich grain.

NanoSIMS offers a potential increase in resolution over ToF-SIMS (100 nm versus 300 nm, in negative polarity), but unlike ToF-SIMS does not collect a complete mass spectrum with each analysis. In practice, the two techniques are highly complementary. A number of regions within the 50 × 50 μm^2 area mapped by ToF-SIMS were chosen for high-resolution mapping using the Cameca NanoSIMS 50 at Washington University in St. Louis, Missouri, USA. These measurements were made by rastering a 16 keV, ~1pA Cs^+ primary ion beam with a diameter of 100 nm across 7 × 7 to 20 × 20 μm^2 areas in 256^2 or 512^2 pixels and detecting secondary electrons (SE), $^{16}O^-$, $^{17}O^-$, $^{18}O^-$, and $^{27}Al^-$ with separate electron multipliers (EMs). In multicollection measurements the mass resolving power (MRP) varies with the detector, but was adjusted sufficiently high to separate isobaric interferences, such as $^{16}O^1H^-$ from $^{17}O^-$ at a MRP of ~6500. A total of 650 μm^2 was studied by NanoSIMS oxygen isotope imaging, entirely within the 2500 μm^2 (50 × 50 μm^2) area that was previously analyzed by ToF-SIMS. An additional NanoSIMS measurement under the same analytical conditions was made on a larger (50 μm) CAI elsewhere in Acfer 094. The O isotopic compositions of regions of interest inside the raster areas were calculated following standardized routines (Stadermann et al. 2005), using the bulk matrix as an internal standard. All δ-values are thus matrix normalized. All errors for isotopic ratios are based on 1σ uncertainties. Silicon isotopes of a 10 × 10 μm^2 sub-area were measured under equivalent analytical conditions, except that the detected species were $^{12}C^-$, $^{27}Al^-$, $^{28}Si^-$, $^{29}Si^-$, $^{30}Si^-$, and SE. A 16 keV O^- beam with a diameter of 300 nm was then used for the measurement of Mg isotopes with parallel detection of $^{12}C^+$, $^{24}Mg^+$, $^{25}Mg^+$, $^{26}Mg^+$, and $^{27}Al^+$ secondary ions in five EMs. Finally, also with a O^- primary beam, the Li isotopic composition of a Li-rich hotspot was measured with detection of $^6Li^+$, $^7Li^+$, and $^{24}Mg^+$ in three separate EMs.

RESULTS AND DISCUSSION

LA-ICP-MS Analysis

The matrix of Acfer 094 was analyzed using LA-ICP-MS, and trace- and minor-element abundances were presented in Bland et al. (2005b). Although the composition of Acfer 094 matrix was not discussed at length by these authors, it offers a useful starting point and aid in interpreting the subsequent higher spatial resolution analyses that are the focus of the current work. As is clear from Fig. 1, the matrix of Acfer 094 is very similar in composition to CM2 matrix. It is slightly enriched in volatiles compared to CM2 bulk, but shows a consistent depletion compared to CI1. From this we can conclude that aqueous alteration on asteroids does not fractionate volatile and moderately volatile elements in chondrite matrix to any substantial degree (since hydrated CM2 matrix is essentially indistinguishable from anhydrous Acfer 094 matrix). The minimal effect of aqueous alteration on chondrite chemistry (with metasomatism largely restricted to ~100 μm zones around chondrules) is discussed in more detail by Bland et al. (2005b).

It is also apparent that Acfer 094 matrix records the same signature of volatile depletion observed in other meteorites and terrestrial planets. This last point is important, as it may suggest that a substantial fraction of “pristine” matrix is thermally processed prior to accretion, and that the composition and mineralogy of matrix phases may offer clues to the nature of this thermal processing, and the mechanism for volatile depletion. An alternative option for producing a depleted matrix composition, suggested by Alexander (2005), is that an undepleted CI1-like composition has been diluted by addition of volatile-poor, refractory-rich material (e.g., chondrule fragments). As Yb is a refractory element, normalizing to CI and Yb (as in Fig. 1) would mask any refractory enrichment. However, normalizing to CI and Mg, we still do not observe the increase in refractory elements that would be expected if the addition of chondrule fragments were producing the observed depletion in volatiles. The abundance of elements with condensation temperatures >1350 K (Lodders 2003), as determined by LA-ICP-MS (Zr, Hf, Sc, Y, Gd, Dy, Ho, Er, Lu, Th, U, Nd, Mo, Sm, Ti, La, Ta, Nb, Yb, Ce, Sr, Be, V, Pt, Rh, Eu), ratioed to CI and Mg, is 1.02 ± 0.03. Conversely, the abundance of elements with condensation temperatures <1000 K is 0.7–0.8 (CV, CO, and CM matrix also shows an absence of refractory enrichment [Bland et al. 2005b; Gordon et al. 2007]). Our LA-ICP-MS analysis shows no detectable enrichment in refractories above CI in Acfer 094 matrix, although we do see a consistent depletion in volatiles. If matrix is volatile-depleted, and if this depletion did not arise from addition of chondrule fragments (high-resolution element mapping (see below) will also constrain the abundance of chondrule-derived material in matrix), then this suggests that matrix was thermally

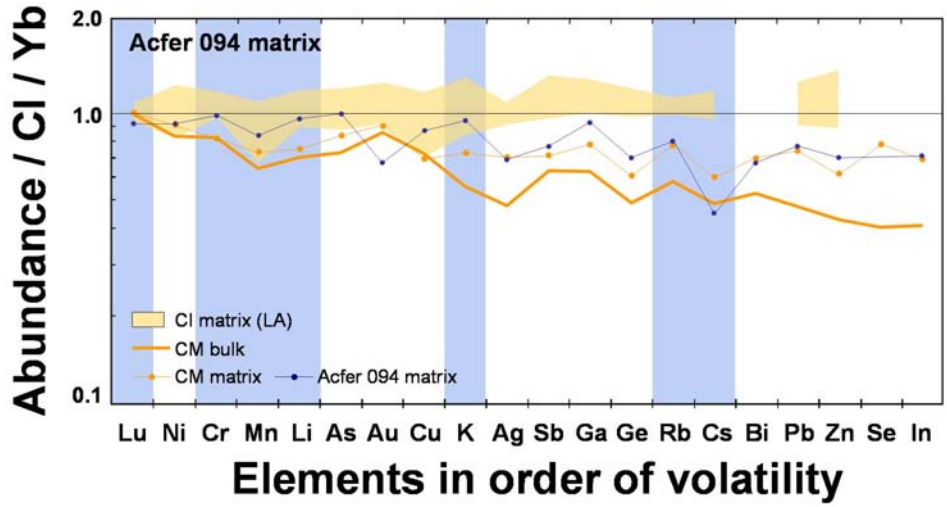

Fig. 1. Trace-element data from LA-ICP-MS analysis of Acfer 094 matrix (Bland et al. 2005b), compared to averaged matrix data from 6 CM chondrites and 2 CI chondrites (Bland et al. 2005b), and averaged bulk data from 7 CM chondrites (Kallemeyn and Wasson 1981). Data are for moderately volatile and volatile elements (Lu and Ni shown for reference), ordered in a sequence of increasing volatility (lithophiles are indicated by the blue bars), and normalized to CI and Yb.

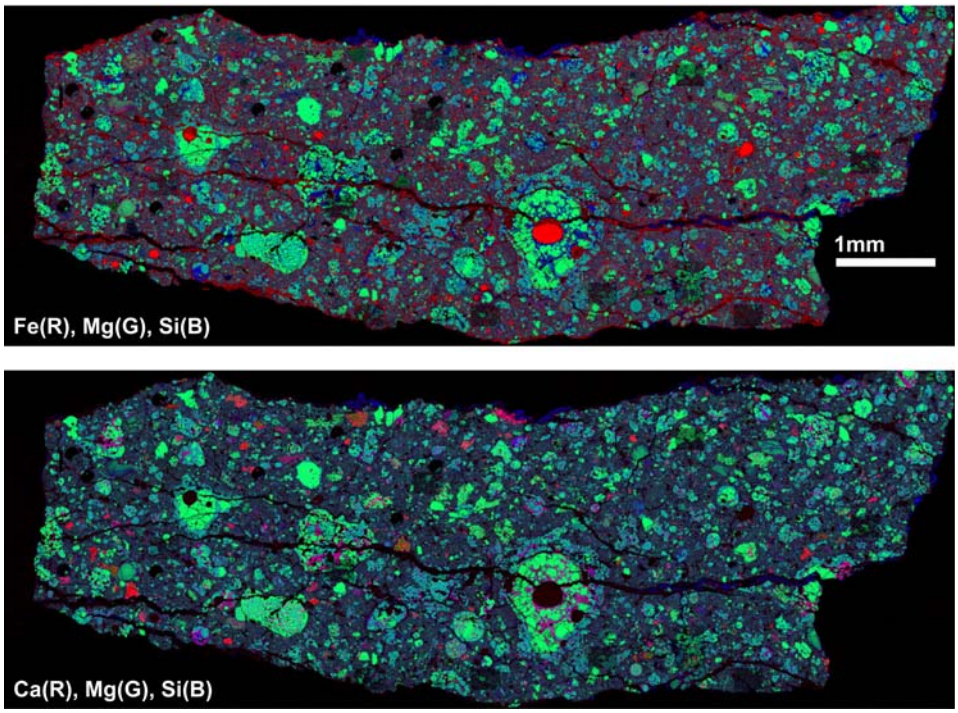

Fig. 2. False-color energy dispersive scanning electron microscope maps of a section of Acfer 094, showing the distributions of Fe, Mg, Si, and Ca (Fe[R], Mg[G], Si[B] at top; Fe[R], Mg[G], Ca[B] at bottom). The original spatial resolution of this EDS map is ~1–2 μm. Macroscopic phases (chondrules, large CAIs, etc.) can be clearly distinguished.

processed. Rather than diluting any depletion (as per two-component models [Anders 1964; Shu et al. 1996; Alexander et al. 2001; Alexander 2005]), chondrite matrix was part of the depletion event(s) that affected the inner solar system. Potentially, the mineralogy of matrix in meteorites that have experienced minimal asteroidal processing can therefore be used to constrain the mechanism for volatile depletion.

SEM-EDS Analysis

A polished thick section of the Acfer 094 meteorite was initially characterized by electron microscopy, which involved complete mapping by energy dispersive spectroscopy at ~1–2 μm spatial resolution. The distributions of Fe, Mg, Si, and Ca are shown in Fig. 2. As noted by

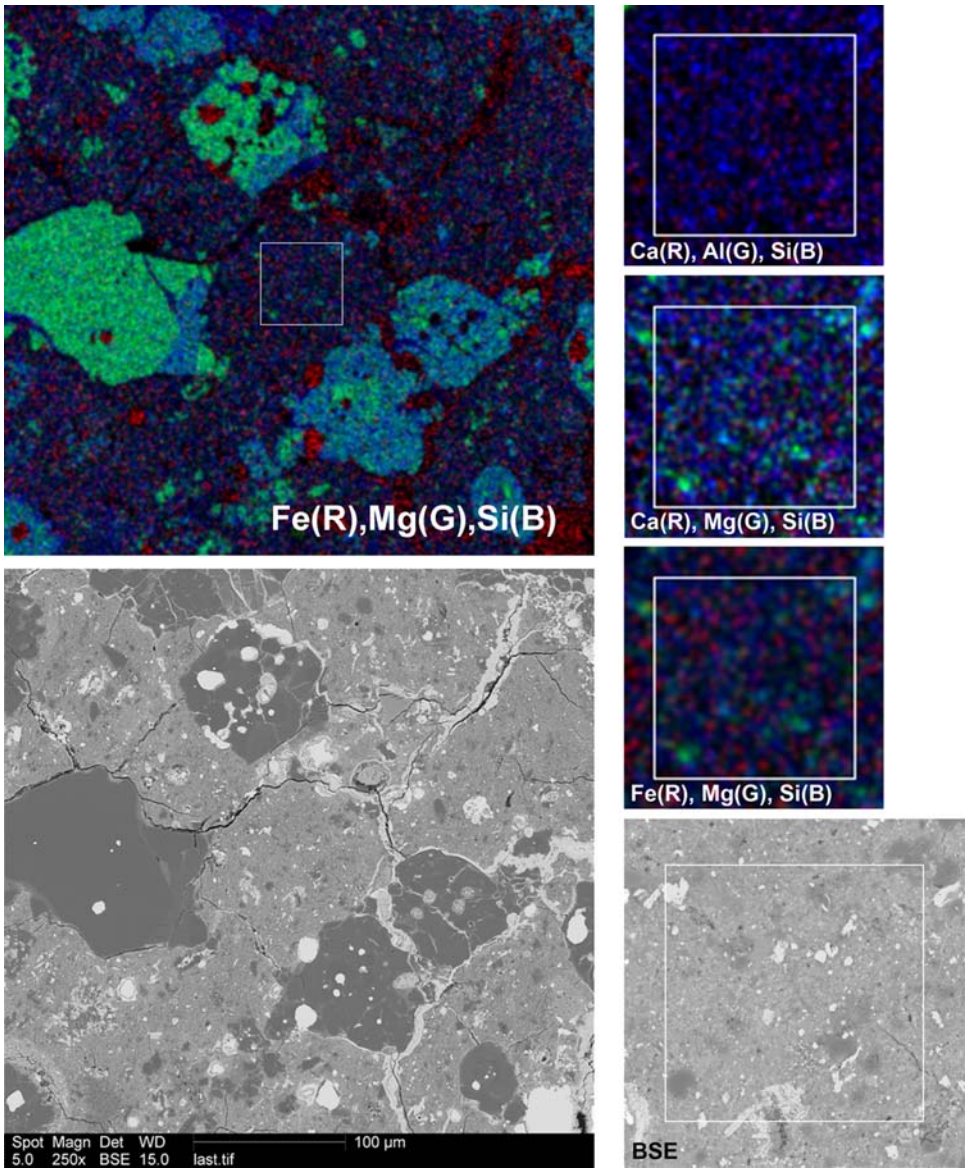

Fig. 3. Energy dispersive scanning electron microscope maps of Acfer 094, showing the distributions of Fe, Mg, and Si in the area of interest as RGB false-color images, and backscattered electron (BSE) images of the same area. The white box indicating the area of interest is 50 × 50 μm^2. It is apparent that within matrix, only the largest (~5 μm) grains can be distinguished using SEM-EDS.

Newton et al. (1995) and Greshake (1997), the dominant phases in Acfer 094 matrix are refractory olivine and pyroxene, as well as sulfide, set in an amorphous groundmass. But it is apparent that even at the maximum spatial resolution (Fig. 3), only the largest matrix grains are visible. To get detailed information on the composition of matrix phases we need to employ additional techniques.

ToF-SIMS Analysis

ToF-SIMS offers a lateral spatial resolution that is approximately an order-of-magnitude improvement on the compositional mapping performed by SEM-EDS. Following SEM analysis, the 50 × 50 μm^2 area of matrix shown in the Fig. 3 area was chosen for a detailed ToF-SIMS elemental study (Fig. 4). A variety of new, minor phases were observed. In the following section we discuss associations for specific elements. The phases expected to condense during equilibrium condensation of a solar gas (Lodders 2003) are listed as a guide in the text, but this is intended only to provide a point of comparison, not to suggest a formation mechanism.

Mg, Si, and Fe

The most common association for Mg, Si, and Fe is in the form of the reddish-orange or mustard-colored material shown in the Mg-Si-Fe red-green-blue (RGB) composite

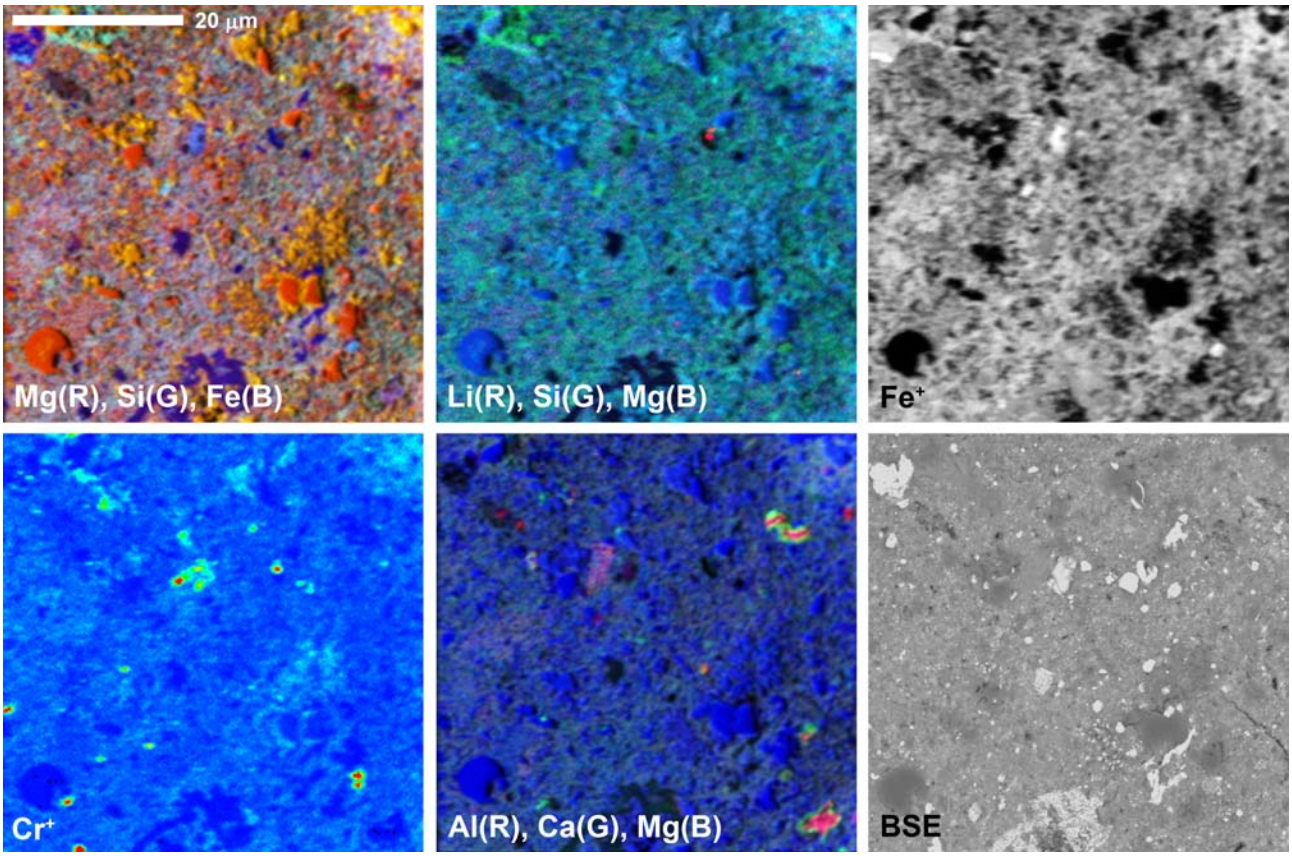

Fig. 4. Selected ToF-SIMS RGB elemental false-color maps of a 50 × 50 μm^2 area in the matrix of Acfer 094. A backscattered electron (BSE) image of the same region is shown for comparison.

secondary ion image (Fig. 4), or the pinkish groundmass. It appears likely that these components correspond to the major components observed by Greshake (1997): olivine, pyroxene, and amorphous groundmass. Greshake (1997) analyzed the amorphous material in Acfer 094 matrix, and observed a major-element composition of approximately 48 wt% SiO_2, 27 wt% FeO, 10 wt% MgO, and 6 wt% NiO, with Al_2O_3 at 3.9 wt%, and CaO at 1.5 wt%. With (relatively) high Mg and Fe, and low Al and Ca, this is manifestly not a typical chondrule glass composition. Our ToF-SIMS data support Greshake's analysis, showing a Fe- and Mg-rich phase, with negligible Ca and Al.

Fe, Ni, and S

Sulfide is commonly Ni-bearing, as observed by Greshake (1997). FeNi metal is also observed, with Ni contents varying significantly across the region of interest.

Na and K

These elements occur together in one region of the mapped area, and are associated with Al, in a Mg- and Fe-poor phase. During equilibrium condensation Na and K are predicted to condense in feldspar, and this may be the likely host here. Alternatively, it is possible that this is a fragment of chondrule mesostasis, although the relatively low abundance of Ca is not consistent with that association.

Li

One Li hotspot is observed, coincident with a Cr feature. Equilibrium condensation would predict Li in forsterite + enstatite. Because the Li hotspot is associated with a grain that is just below the spatial resolution for ToF-SIMS, we cannot fully exclude the possibility that the Li and Cr are hosted in an olivine. However, this would hardly be consistent with the qualitative finding of an almost Si-free pocket, containing the Li,Cr-rich grain, surrounded almost completely by a S-rich phase, probably a sulfide (Fig. 5). With the LiCr grain at the limit of ToF-SIMS spatial resolution, it is difficult to determine whether it contains any significant Fe, Mg, or Ni. However, judging from the profile across it, it is rather pure LiCr or LiCr oxide. Our best estimate is Li:Cr = 1:6 in this grain.

Mn

We would expect Mn in forsterite + enstatite, and in Acfer we do find it co-located with Mg and Si. We also observe a Mn-rich phase with significantly less Si, which appears to be intergrown with a Na- and K-rich phase.

Cr

Based on equilibrium condensation, we would expect Cr in an Fe alloy. Abundant Cr hotspots are observed in Acfer 094 matrix (Fig. 4). With the exception of the anomalous LiCr grain, the dominant chemistry appears to be Fe and Cr in approximately equal proportions (with minimal oxygen): a Cr,Fe-alloy. Interestingly, Keller and Takayama (2005) have recently observed grains with a similar element association within amorphous silicates in IDPs.

F and Cl

Equilibrium condensation predicts apatite and sodalite, respectively, as host phases for these elements. In Acfer 094 these elements are associated with a framboidal Fe oxyhydroxide, possibly ferrihydrite (Greshake 1997) or goethite. Our interpretation is that these phases are the result of terrestrial weathering.

Ca and Al

ToF-SIMS revealed a number of small Ca-Al-rich inclusions (Fig. 4). The larger members of this group of objects (2–5 μm) are clearly zoned in Ca and Al, with what appear to be pure Al, Ca-free (possibly corundum) cores, surrounded by Al, Ca-containing (possibly hibonite) rims. Smaller objects are also observed, with sizes down to the limit of ToF-SIMS resolution, but it is not possible to determine whether they show any zonation. These μCAIs were first reported in the matrix of Acfer 094 by Bland et al. (2005a) and Nakamura et al. (2005), both groups observing a similar compositional association. Based on observations such as their size distribution (Nakamura et al. 2005), and the fact that continuous Al, Ca-containing rims are observed around pure Al, Ca-free cores (Bland et al. 2005a), it is apparent that these μCAIs are a distinct population, not fragments of larger CAIs. Nakamura et al. (2005, 2006, 2007) have observed that some pure Al, Ca-free grains are found as aggregates, and have used this fact to constrain conditions during condensation. EBSD analysis by Nakamura et al. (2007) confirms that this phase is corundum.

NanoSIMS Analysis

The oxygen isotopic composition of specific areas (e.g., the μCAIs observed using ToF-SIMS) was mapped using the NanoSIMS. NanoSIMS analyses also constrained the Li-isotope composition of the Li hotspot, and determined the Mg and Si isotopic compositions for specific areas of the sample.

μCAIs

Nakamura et al. (2005) performed oxygen isotopic ion imaging using an IMS1270 on a region of Acfer 094 matrix containing μCAIs. They noted that μCAIs had a similar composition to larger CAIs, although specific data were not presented. We used the NanoSIMS in imaging mode to map

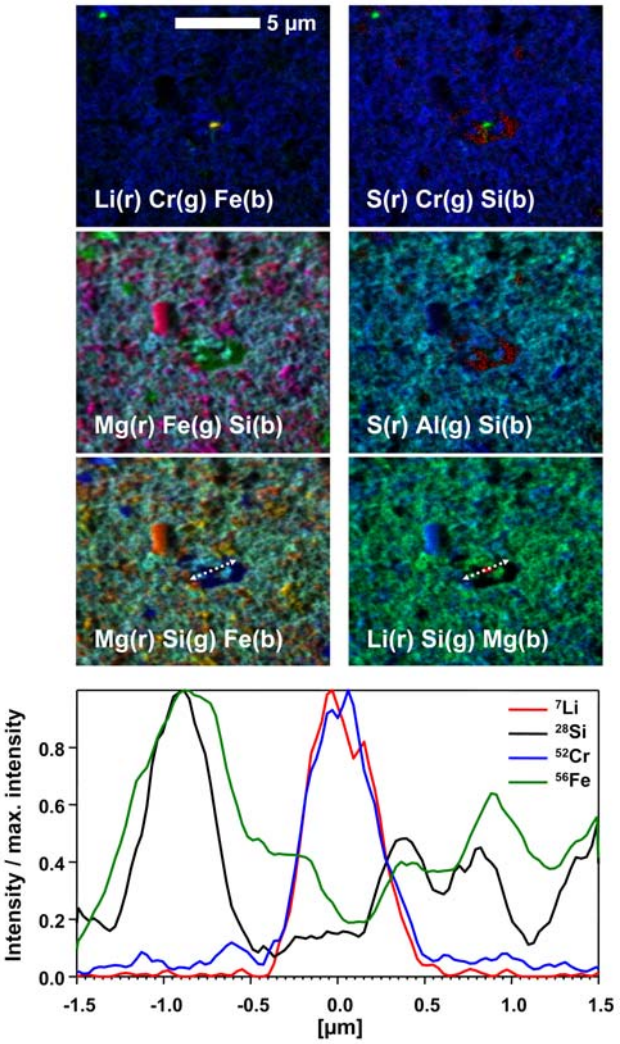

Fig. 5. ToF-SIMS profile across the Li-enriched grain. The position of the one-dimensional profile is indicated in the bottom set of three-color maps. The secondary ion intensities have been normalized within the given range of the profile.

oxygen isotopes at high spatial resolution in our sample (Fig. 6). Note that these data are normalized to the surrounding Acfer 094 matrix. Given that matrix in anhydrous carbonaceous chondrites is typically 2–3‰ heavier than the bulk meteorite (Clayton and Mayeda 1999), an Acfer 094 bulk composition with $\delta^{17}O$ at −3.91‰ and $\delta^{18}O$ at 1.17‰ (Clayton and Mayeda 1999) would suggest a matrix composition in the vicinity of $\delta^{17}O$ at −1.4‰ and $\delta^{18}O$ at 3.7‰.

Oxygen isotopic mapping by NanoSIMS (Fig. 6) revealed that two of the three μCAIs (b and c) have isotopically normal oxygen ($\delta^{17}O$: −2 ± 4‰, $\delta^{18}O$: 6 ± 3‰; and, $\delta^{17}O$: −11 ± 12‰, $\mu^{18}O$: 6 ± 5‰, respectively), and that the third (μCAI a) is more ^{16}O-rich ($\delta^{17}O$: −28 ± 3‰; $\delta^{18}O$: −29 ± 1‰), although not as ^{16}O-rich as is typical for larger CAIs. The "classical" (i.e., larger) CAIs previously described

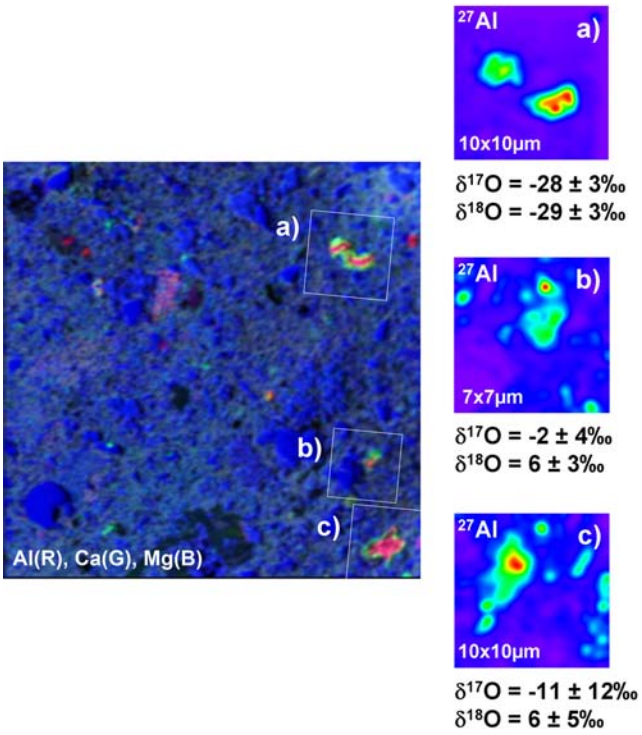

Fig. 6. NanoSIMS analysis to define the oxygen isotopic composition of three μCAIs in the area analyzed by ToF-SIMS. A ToF-SIMS map for Al, Ca, and Mg identifies the position of the μCAIs. In addition to analyzing for oxygen isotopes, ^{27}Al was imaged to confirm the locations of the CAIs in the NanoSIMS maps. In the NanoSIMS false color images on the right, the highest Al concentrations are shown in red.

in Acfer 094 are in the size range 40–500 μm (Weber 1995; Krot et al. 2004) and overwhelmingly have ^{16}O-rich oxygen compositions (Fagan et al. 2003; Krot et al. 2004). As it appeared possible that the lack of a strong ^{16}O-enrichment observed in the μCAIs could be due to secondary alteration at the micron-scale (either pre- or post-accretion), we also performed oxygen mapping at the contact between a larger CAI (50 μm) and matrix. This analysis showed that the large CAI was ^{16}O-rich ($\delta^{17}O$: −39 ± 2‰, $\delta^{18}O$: −42 ± 1‰) right up to the contact with matrix, suggesting that the O isotopic compositions measured in the μCAIs are not an alteration effect. It appears, therefore, that in addition to the reasons outlined above, μCAIs may also be a distinct population in terms of their oxygen isotopic compositions.

We also looked for ^{26}Mg enrichments in the μCAIs that would be an indication of the in situ decay of ^{26}Al, but did not find any detectable anomalies. However, due to the fact that neighboring phases were relatively Mg rich, and because of the lower spatial resolution of the required O^- beam, we were not able to clearly separate the Mg signal of the μCAI from that of the surrounding material. This made it impossible to measure any ^{26}Mg enrichment, even if ^{26}Al were originally present in the sample.

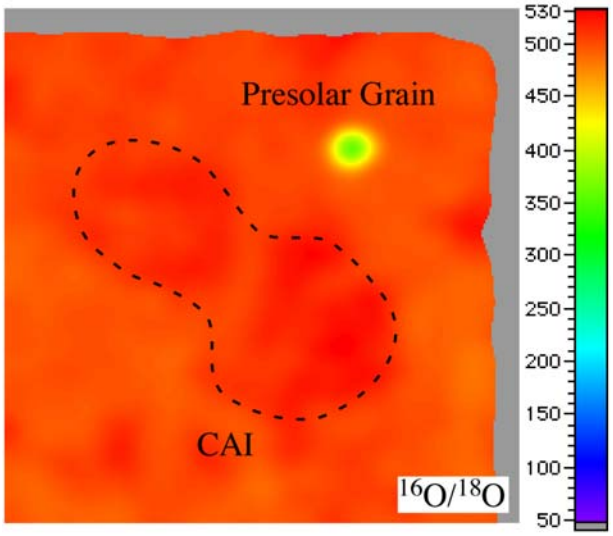

Fig. 7. False-color image of the $^{16}O/^{18}O$ distribution in a 10 × 10 μm^2 area of Acfer 094. The approximate outline of a μCAI (cf. Fig. 6a) is shown. On this map the composition of the CAI ($^{16}O/^{18}O \approx 519$) is difficult to discern from the average, normal background ($^{16}O/^{18}O \approx 499$), while the presolar grain stands out as being significantly ^{18}O-rich. No data are available from the gray area.

Lithium-Enriched Grain

From our NanoSIMS measurements, it is apparent that the Li grain is significantly larger than was suggested by the ToF-SIMS analysis (in the region of 1 μm). It is likely that this discrepancy is related to the nature of the SIMS technique—SIMS is a dynamic measurement technique. It is conceivable that a small part of the Li grain was exposed during the ToF-SIMS measurements (the tip of the iceberg) and that the bulk of the grain was only excavated during the NanoSIMS measurements.

The unusual composition of this grain raised the possibility that it might be presolar in origin. In terms of its isotopic composition, the Li-enriched grain is (within 2σ) the same as the surrounding matrix. Due to the relatively low signal, we cannot define the composition on a permil level, but there is clearly no Li-isotopic anomaly in this particle at the 10% or greater level. We note, however, that estimates of the Li-isotope ratio in the interstellar medium, based on astronomical observations, are in excellent agreement with the solar system (meteoritic) value (Howarth et al. 2002). Thus, the absence of a Li-isotope anomaly is not necessarily unexpected, even if the grain does have a presolar origin.

Presolar Grain

As discussed above, we used the NanoSIMS to determine the O-isotopic variations in the μCAIs which were identified by ToF-SIMS imaging. During the course of these measurements, we discovered an ^{18}O-rich presolar grain. Since the area of the presolar grain had previously been analyzed by ToF-SIMS, we were able to correlate elemental

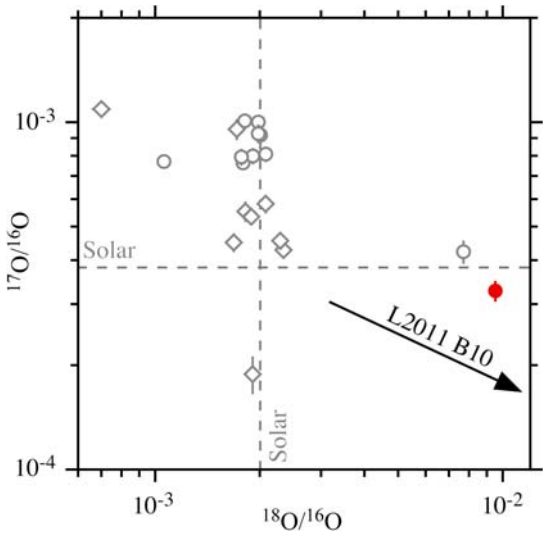

Fig. 8. Three-isotope plot of the O-isotopic compositions of presolar silicates in Acfer 094. The ^{18}O-rich grain from this study is shown as a full circle. For comparison, the results from previous studies of Acfer 094 are shown as diamonds (Nguyen and Zinner 2004) and open circles (Mostefaoui and Hoppe 2004). In most cases, the 1σ error bars are smaller than the symbols. The composition of an even more ^{18}O-rich grain in interplanetary dust particle L2011 B10 (Messenger et al. 2005) is indicated for comparison.

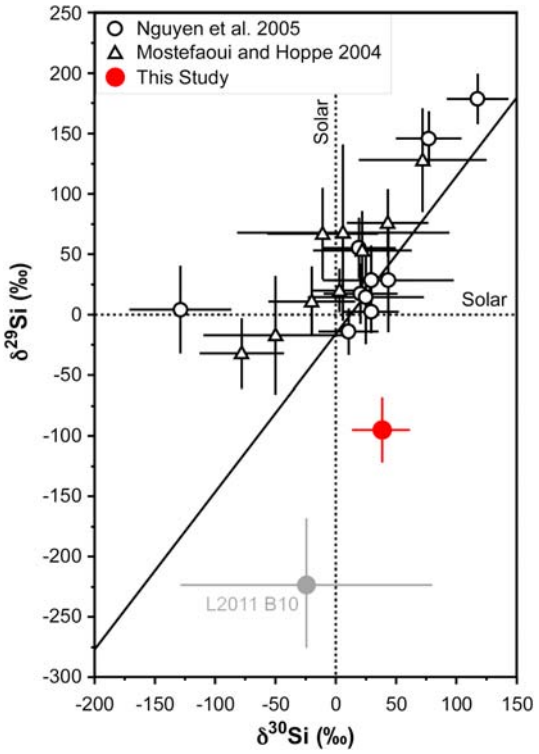

Fig. 9. Silicon three-isotope plot of the compositions of previously identified presolar silicates from meteorites (Nguyen et al. 2005; Mostefaoui and Hoppe 2004) and of the presolar silicate grain from this study. Most of the earlier data fall near or slightly to the left of the "mainstream SiC" correlation line, which likely reflects the spread of initial Si isotopic compositions in the parent stars. Also shown for comparison is the composition of the supernova grain in interplanetary dust particle L2011 B10 (Messenger et al. 2005).

and isotopic data to aid in a mineralogical identification of the particle.

The area with both the μCAI (which is the same one shown in Fig. 6a) and the presolar grain is shown in Fig. 7. Note that smoothing of the false-color image leads to an increase in the apparent size and a dilution of the composition of small features, i.e., the presolar grain. The level of image smoothing performed, however, is required for the analysis of the CAI. A more detailed data analysis of the area shows that the presolar grain has a diameter of 250 nm. Its isotopic composition is $^{18}O/^{16}O = (9.52 \pm 0.12) \times 10^{-3}$ and $^{17}O/^{16}O = (3.28 \pm 0.23) \times 10^{-4}$. Expressed in delta notation, this composition is $\delta^{18}O = 3750‰$ and $\delta^{17}O = -139‰$. The presolar grain is in no way related to the nearby μCAI.

To determine the composition of the presolar grain, we can use information from the NanoSIMS measurement and the preceding ToF-SIMS characterization. The NanoSIMS Al data clearly indicate that the ^{18}O-rich area cannot be an Al-bearing mineral. Since the O intensity is similar to surrounding areas, the presolar grain may be a silicate. To use the ToF-SIMS data for characterization, it is necessary to register the elemental and isotope ratio images on a sub-micrometer scale. Owing to the lack of distinct reference points in the image, the fact that the size of the presolar grain is close to the spatial resolution of the ToF-SIMS technique, and the slight depth difference analysed by the two methods (see above), this registration is only partially successful. The area in the immediate vicinity of the presolar grain has a composition that is dominated by O, Fe, Si, and with smaller amounts of Mg. Within this region of interest the secondary ion intensities were reduced using silicate relative sensitivity factors. While the atom fractions relative to Si are not strictly stoichiometric, and ToF-SIMS is not typically used for major element mineral chemistry, the presolar grain appears to most closely resemble Fe-bearing olivine in its major chemistry.

Given the total matrix area analyzed in this phase of the study (650 μm^2) and the established abundance of presolar silicates in Acfer 094 (176 ppm) (Nguyen et al. 2005; Nguyen et al. 2007), it is actually not surprising to find a presolar grain in the analyzed area. The O isotopic composition of the newly discovered presolar silicate grain is shown in Fig. 8 together with those of previously observed silicates in Acfer 094. This grain is the most ^{18}O-rich silicate found so far in meteorites, although its O isotopic composition is in the same region (group 4; Nittler et al. 1997) of the three-isotope plot as a presolar silicate (pyroxene) found by Mostefaoui and Hoppe (2004). An even more ^{18}O-enriched olivine grain (which TEM showed to be unusually Fe-rich) was previously found in an interplanetary dust particle, and for that presolar grain a supernova origin was asserted (Messenger et al. 2005). However, the origin of most ^{18}O-rich oxide and silicate grains

remains unclear. While both supernovae and asymptotic giant branch (AGB) stars have been suggested as possible sources for some of these grains (Nittler et al. 1997; Choi et al. 1998), the extreme ^{18}O-enrichment of the particle in this study points toward a supernova origin. In fact, low-density presolar graphite grains with origins in type II supernovae frequently exhibit similar ^{18}O-enrichment with fairly normal $^{17}O/^{16}O$ ratios (Travaglio et al. 1999). As summarized by Messenger et al. (2005), large enrichments in $^{18}O/^{16}O$ may be produced in the He/C shell during He burning. Although this region is C-rich, the $^{18}O/^{16}O$ ratio is so high that only a small amount of this material needs to be mixed in with O-rich material to produce a large observed anomaly.

The Si composition of the ^{18}O-rich grain was determined as $^{29}Si = (–96 \pm 27)‰$ and $\delta^{30}Si = (38 \pm 24)‰$, which is distinctly different from the composition of other presolar silicates (Fig. 9) for which an AGB star origin is assumed (Nguyen et al. 2005; Nguyen et al. 2007; Mostefaoui and Hoppe 2004). The Si isotopic compositions of supernova graphite also generally fall close to the "mainstream SiC" correlation line (Fig. 9), although with a much wider range of ^{28}Si abundances (Travaglio et al. 1999). The observed Si isotopic composition of the ^{18}O-rich grain is similar to that which is seen in SiC grains of type Z, where such compositions are explained as a combination of two processes: the galactic evolution of Si isotopes, and AGB mixing during third dredge-up events (Zinner et al. 2006). However, as mentioned above, AGB stellar evolution cannot account for the extreme ^{18}O-enrichment observed in this grain. With two origin scenarios (AGB star and type II supernova) to consider and the Si and O isotopic data seemingly suggesting different interpretations, we believe that a supernova origin is more likely for the presolar silicate grain from this study. It should be noted that the ^{18}O-rich supernova olivine grain found in an interplanetary dust particle (Messenger et al. 2005) also has a Si isotopic composition that is more ^{30}Si-rich than those of typical supernova graphites. Overall, the Si and O isotopic compositions of our grain are rather similar to that described by Messenger et al. (2005), for which a supernova origin was proposed.

CONCLUSIONS

The combination of techniques applied here provides a powerful new window on the mineralogy and composition of chondrite matrix. This analysis has significantly expanded the suite of phases observed in Acfer matrix, identified an unusual set of μCAIs, an anomalous Cr,Li-bearing phase, and the most ^{18}O-rich silicate found so far in meteorites. Matrix in Acfer 094 is highly unequilibrated and heterogeneous at all spatial scales, down to the limits of NanoSIMS resolution.

The high-resolution element mapping and LA-ICP-MS analyses that we present here can be seen as complementary to earlier TEM studies (e.g., Greshake 1997). Both our analyses, and those of Greshake (1997), suggest that fragmental material (clastic material derived from chondrules or CAIs) makes up a negligible proportion of matrix. Evidence to support this suggestion comes from a variety of sources: failure to observe chondrule-derived phases in matrix; failure to observe any refractory enrichment in matrix; failure to observe fragmental CAI material (although μCAIs are observed, these objects show complete zoning, and are clearly intact, not fragments of larger CAIs).

Does the observed matrix mineralogy help in constraining models for volatile depletion? Currently the data from Acfer 094 are equivocal. We observe carrier phases for several elements consistent with conditions that approach those expected during equilibrium condensation; others (e.g., Li) are not; and an amorphous groundmass (Greshake 1997) suggests disequilibrium condensation. Further work is required to address this important question.

Acknowledgments–P. A. B. thanks the Royal Society and the Particle Physics and Astronomy Research Council (PPARC) for their support. This work was funded under PPARC grant PPA/G/S/2003/00071. The NanoSIMS work was partially supported by NASA grant NNG05GJ66G to Frank Stadermann. We also thank Ann Nguyen for allowing us to use her section of Acfer 094 for the analysis of the large CAI. The final manuscript benefited greatly from comments by Conel Alexander, Sasha Krot, Scott Messenger, and Larry Nittler.

Editorial Handling—Dr. Larry Nittler

REFERENCES

Alexander C. M. O'D., Boss A. P., and Carlson R. W. 2001. The early evolution of the inner solar system: A meteoritic perspective. *Science* 293:64–68.

Alexander C. M. O'D. 2005. Re-examining the role of chondrules in producing the elemental fractionations in chondrites. *Meteoritics & Planetary Science* 40:943–965.

Anders E. 1964. Origin, age, and composition of meteorites. *Space Science Reviews* 3:583–714.

Bland P. A., Alard O., Gounelle M., and Rogers N. W. 2003. Trace element variability in carbonaceous chondrite matrix (abstract #1750). 34th Lunar and Planetary Science Conference. CD-ROM.

Bland P. A., Alard O., Gounelle M., Benedix G. K., Kearsley A. T., and Rogers N. W. 2004. Volatile and moderately volatile trace element composition of chondrules and matrix from CM chondrites: Implications for chondrule formation (abstract #1737). 35th Lunar and Planetary Science Conference. CD-ROM.

Bland P. A., Rost D., Vicenzi E. P., Stadermann F. J., Floss C., Fries M., Steele A., Benedix G. K., Lee M. R., Watt L. E., and Kearsley A. T. 2005a. Trace element carrier phases in primitive chondrite matrix: Implications for volatile element fractionation in the inner solar system (abstract #1841). 36th Lunar and Planetary Science Conference. CD-ROM.

Bland P. A., Alard O., Benedix G. K., Kearsley A. T., Menzies O. N., Watt L. E., and Rogers N. W. 2005b. Volatile fractionation in the early solar system and chondrule/matrix complementarity.

Proceedings of the National Academy of Sciences 102:13,755–13,760.

Cassen P. 1996. Models for the fractionation of moderately volatile elements in the solar nebula. *Meteoritics & Planetary Science* 31: 793–806.

Cassen P. 2001. Nebular thermal evolution and the properties of primitive materials. *Meteoritics & Planetary Science* 36:671–700.

Choi B.-G., Huss G. R., Wasserburg G. J., and Gallino R. 1998. Presolar corundum and spinel in ordinary chondrites: Origins from AGB stars and a supernova. *Science* 282:1284–1289.

Clayton R. N. and Mayeda T. K. 1999. Oxygen isotope studies of carbonaceous chondrites. *Geochimica et Cosmochimica Acta* 63: 2089–2104.

Fagan T. J., Krot A. N., and Yurimoto H. 2003. Petrology and oxygen isotope compositions of refractory inclusions from Acfer 094 (abstract #1274). 34th Lunar and Planetary Science Conference. CD-ROM.

Flynn G. J., Keller L. P., and Sutton S. R. 2004. Sub-micrometer scale minor element mapping in interplanetary dust particles: A test for stratospheric contamination (abstract #1334). 35th Lunar and Planetary Science Conference. CD-ROM.

Gordon S. H., Hammond S. J., Rogers N. W., Charlier B. L. A., and Bland P. A. 2007. Constraints on volatile depletion from chondrite matrix (abstract #1819). 38th Lunar and Planetary Science Conference. CD-ROM.

Greshake A. 1997. The primitive matrix components of the unique carbonaceous chondrite Acfer 094: A TEM study. *Geochimica et Cosmochimica Acta* 61:437–452.

Howarth I. D., Price R. J., Crawford I. A., and Hawkins I. 2002. A VAPID analysis of interstellar lithium in the ζ Oph sightline. *Monthly Notices of the Royal Astronomical Society* 325:267–274.

Huss G. R., Meshik A. P., Smith J. B., and Hohenberg C. M. 2003. Presolar diamond, silicon carbide, and graphite in carbonaceous chondrites: Implications for thermal processing in the solar nebula. *Geochimica et Cosmochimica Acta* 67:4823–4848.

Kallemeyn G. W. and Wasson J. T. 1981. The compositional classification of chondrites. I—The carbonaceous chondrite groups. *Geochimica et Cosmochimica Acta* 45:1217–1230.

Keller L. P. and Takayama A. 2005. Transition element (Fe, Cr, and Mn) oxidation states recorded in primitive interplanetary dust (abstract). Workshop on Oxygen in the Earliest Solar System. p. 24.

Krot A. N., Fagan T. J., Keil K., McKeegan K. D., Sahijpal S., Hutcheon I. D., Petaev M. I., and Yurimoto H. 2004. Ca,Al-rich inclusions, amoeboid olivine aggregates, and Al-rich chondrules from the unique carbonaceous chondrite Acfer 094: I. mineralogy and petrology. *Geochimica et Cosmochimica Acta* 68:2167–2184.

Lodders K. 2003. Solar abundances and condensation temperatures of the elements. *The Astrophysical Journal* 591:L1220–L1247.

Messenger S., Keller L. P., and Lauretta D. S. 2005. Supernova olivine from cometary dust. *Science* 309:737–741.

Mostefaoui S. and Hoppe P. 2004. Discovery of abundant in situ silicate and spinel grains from red giant stars in a primitive meteorite. *The Astrophysical Journal* 613:L149–L152.

Nagashima K., Krot A. N., and Yurimoto H. 2004. Stardust silicates from primitive meteorites. *Nature* 428:921–924.

Nakamura T. M., Sugiura N., Kimura M., Miyazaki A., and Krot A. N. 2005. Corundum and corundum-hibonite grains discovered by cathodoluminescence in the matrix of Acfer 094 meteorite (abstract #1249). 36th Lunar and Planetary Science Conference. CD-ROM.

Nakamura T. M., Sugiura N., Kimura M., Miyazaki A., and Krot A. N. 2006. Condensation and accretion of corundum and corundum-hibonite grains in the solar nebula (abstract #1249). 37th Lunar and Planetary Science Conference. CD-ROM.

Nakamura T. M., Sugiura N., Kimura M., Miyazaki A., and Krot A. N. 2007. Condensation and aggregation solar of corundum and corundum-hibonite grains. *Meteoritics & Planetary Science*. This issue.

Newton J., Bischoff A., Arden J. W., Franchi I. A., Geiger T., Greshake A., and Pillinger C. T. 1995. Acfer 094, a uniquely primitive carbonaceous chondrite from the Sahara. *Meteoritics* 30:47–56.

Nguyen A. and Zinner E. 2004. Discover of ancient silicate stardust in a meteorite. *Science* 303:1496–1499.

Nguyen A. N., Zinner E., and Stroud R. M. 2005. Continued characterization of presolar silicate grains from the Acfer 094 carbonaceous chondrite (abstract #2196). 36th Lunar and Planetary Science Conference. CD-ROM.

Nguyen A. N., Stadermann F. J., Zinner E., Stroud R. M., Alexander C. M. O'D., and Nittler L. R. 2007. Characterization of presolar silicate and oxide grains in primitive carbonaceous chondrites. *The Astrophysical Journal* 656:1223–1240.

Nittler L. R., Alexander C. M. O'D., Gao X., Walker R. M., and Zinner E. 1997. Stellar sapphires: The properties and origins of presolar Al_2O_3 in meteorites. *The Astrophysical Journal* 483: 475.

Nuth J. A. III, Brearley A. J., and Scott E. R. D. 2005. Microcrystals and amorphous material in comets and primitive meteorites: Keys to understanding processes in the early solar system. In *Workshop on Chondrites and the Protoplanetary Disk*, edited by Krot A. N., Scott E. R. D., and Reipurth B. Honolulu: University of Hawai'i at Manoa. SOEST Publication No. 04-03. pp. 675–700.

Shu F. H., Shang H., and Lee T. 1996. Toward an astrophysical theory of chondrites. *Science* 271:1545–1552.

Stadermann F. J., Floss C., Bland P. A., Vicenzi E. P., and Rost D. 2005. An oxygen-18 rich presolar silicate grain from the Acfer 094 meteorite: A NanoSIMS and ToF-SIMS study (abstract #2004). 36th Lunar and Planetary Science Conference. CD-ROM.

Stadermann F. J., Croat T. K., Bernatowicz T. J., Amari S., Messenger S., Walker R. M., and Zinner E. 2005. Supernova graphite in the NanoSIMS: Carbon, oxygen and titanium isotopic compositions of a spherule and its TiC subcomponents. *Geochimica et Cosmochimica Acta* 69:177–188.

Stephan T. 2002. TOF-SIMS analysis of heavy-nitrogen-carrying phases in interplanetary dust (abstract #1352). 33rd Lunar and Planetary Science Conference. CD-ROM.

Travaglio C., Gallino R., Amari S., Zinner E., Woosley S., and Lewis R. S. 1999. Low-density graphite grains and mixing in type II supernovae. *The Astrophysical Journal* 510:325–354.

Weber D. 1995. Refractory inclusions from the carbonaceous chondrite Acfer 094 (abstract). *Meteoritics* 30:595–596.

Wulf A.V., Palme H., and Jochum P. 1995. Fractionation of volatile elements in the early solar system: Evidence from heating experiments on primitive meteorites. *Planetary and Space Science* 43:451–468.

Wasson J. T. and Chou C.-L. 1974. Fractionation of moderately volatile elements in ordinary chondrites. *Meteoritics* 9:69–84.

Yin Q-Z. 2004. From dust to planets: The tale told by moderately volatile elements. In *Workshop on Chondrites and the Protoplanetary Disk*, edited by Krot A. N., Scott E. R. D., and Reipurth B. Honolulu: University of Hawai'i at Manoa. SOEST Publication No. 04-3. pp. 227–288.

Zinner E., Nittler L. R., Gallino R., Karakas A. I., Lugaro M., Straniero O., and Lattanzio J. C. 2006. Silicon and carbon isotopic ratios in AGB stars: SiC grain data, models, and the galactic evolution of the Si isotopes. *The Astrophysical Journal* 650:350–373.